8

Influence on Earthquake Distributions in Slabs from Bimaterial Shear Heating

Byung-Dal So[1] and David A. Yuen[2]

ABSTRACT

The deviatoric stress regime inside subducting slabs plays an essential role in explaining the distributions of deep focus earthquakes. The relationship between the level of deviatoric stress and aseismic zone (i.e., 300 km to 450 km deep) is not well understood. We suggest that shear heating around the 410 km two-phase coexistence loop (i.e., olivine and spinel) may reduce the deviatoric stress level, and then can reduce the tendency toward transformational faulting. The phase loop makes it possible for a reduction in elastic modulus and consequently act as the bimaterial interface for providing intense shear heating within the loop. When the ratio in elastic moduli between the phase loop and surrounding region is larger than ~2, the stress drop is more than ~0.4 GPa in the phase loop. A localized zone with a low deviatoric stress level represents a new concept in subduction dynamics and may be able to explain the aseismic zone.

8.1. INTRODUCTION

The origin and spatial distribution of deep focus earthquakes (DFEs) within subducting slabs is an important issue in geophysics. In the past, people have proposed various mechanisms for understanding how DFEs occur within deep-subducting slabs where the normal brittle failure is not a preferable regime due to extremely high confining pressure. The most widely discussed mechanisms include: dehydrational embrittlement [e.g., *Meade and Jeanloz*, 1991; *Jung et al*., 2004], transformational faulting related with the olivine-spinel phase transition [e.g., *Green and Brunley*, 1989; *Kirby et al*., 1996], and the slab melting by shear heating [e.g., *Ogawa*, 1987; *John et al*., 2009] around the preexisting weak zone [*Chen and Wen*, 2015], and the differential volume contraction between the subductin gcrust and mantle lithosphere [*Liu and Zhang*, 2015]. Since slabs extending ahead of the Wadati-Benioff zones are clearly observed using seismic tomography imaging [e.g., *Fukao et al*., 2001], we may deduce that the DFEs must be continuously active along the subducting slab. However, most subducting slabs have a peculiar spatial distribution related to the depth of seismic activity. The seismically active regions are divided into two different zones, from the top to 300 km deep and from 450 km deep to the 660-km phase boundary. On the other hand, between 300 km and 450 km of depth, no or few DFEs are detected [*Sykes*, 1966; *Isacks et al*., 1968; *Houston*, 2007]. This pattern raises the question of why a zone of weak seismicity exists between two seismically active zones in spite of continuously increasing pressure and temperature over these depths [*Ji and Salisbury*, 1993; *Frohlich*, 2006; *Myhill*, 2013].

Two possible mechanisms for the lack of DFEs at depths of 300–450 km (hereafter, we use the acronym ASZ for this aseismic zone) have been suggested. One is the lack of hydrous minerals that can be dehydrated

[1]*Research Institute of Natural Sciences, Chungnam National University, Daejeon, South Korea*

[2]*School of Environment Studies, China University of Geosciences, Wuhan, China; Minnesota Supercomputing Institute and Department of Earth Sciences, University of Minnesota, Minneapolis, Minnesota, USA*

Subduction Dynamics: From Mantle Flow to Mega Disasters, Geophysical Monograph 211, First Edition.
Edited by Gabriele Morra, David A. Yuen, Scott D. King, Sang-Mook Lee, and Seth Stein.

under the pressure-temperature condition of the ASZ [*Green et al.*, 2010]. The other is that the olivine-spinel phase transition, which should occur at around the 410-km phase boundary and can cause DEFs through transformational faulting, is delayed due to sluggish kinetics until the depth of ~500 km due to a relatively low temperature in the core of the slab [e.g., *Iidaka and Suetsugu*, 1992]. However, in recent studies, low- (i.e., olivine) and high- (i.e., spinel) pressure polymorphs can coexist around the phase boundary in the subducting slab [*Sung and Burns*, 1976; *Rubie and Ross II*, 1994]. If there is a coexistence of olivine and spinel in the ASZ, this should explain why no DFEs are shown in the ASZ even though the olivine-spinel phase transition is ongoing in the ASZ. Based on experimental studies [e.g., *Schubnel et al.*, 2013], the DEFs by the transformational faulting require large deviatoric stresses (i.e., 1–2 GPa). We may speculate that the deviatoric stress is decreased by additional mechanisms. Shear heating can be the most efficient process for reducing the deviatoric stress [*Peacock et al.*, 1994; *Tackley*, 1998; *Gerya et al.*, 2004]. Through the shear heating, the deviatoric stress around the shear zone can be relaxed by the release of the stored strain-energy as a form of thermal energy [*Schmalholz and Podladchikov*, 2013]. We need now to address which mechanism may induce intense shear heating at this depth inside the slab.

The coexistence of low- and high-pressure polymorph is known as the phase loop [*Jackson and Anderson*, 1970] (see Figure 8.1). Recent experimental mineral physics research on the phase loop, which is associated with the olivine-spinel phase transition, has established that compressional waves are reduced by more than ~40%, corresponding to a ~70% reduction in the effective bulk moduli [*Li and Weidner*, 2008]. Moreover, the elastic shear modulus can also be significantly softened in the phase loop [*Ricard et al.*, 2009], as confirmed in the study by *Li and Weidner* [2008]. This finding has inspired us to recognize that a visible bimaterial interface, which refers to a boundary with a large contrast in elastic moduli, is present in the slab around the 410-km phase boundary. It has been well understood that bimaterial property in shear modulus can trigger shear instability with a preferred propagation orientation [*Ben-Zion and Shi*, 2005; *Ampuero and Ben-Zion*, 2008]. Recently, *So et al.* [2012] argued that larger contrasts in shear moduli between two attached lithospheres generate more energetic shear heating around the interface. In this paper, we numerically investigate how shear heating from the bimaterial instability at the phase loop impacts the thermal structure of the subducting slab. Furthermore, we discuss the dynamical implications for the lack of DFEs in the ASZ.

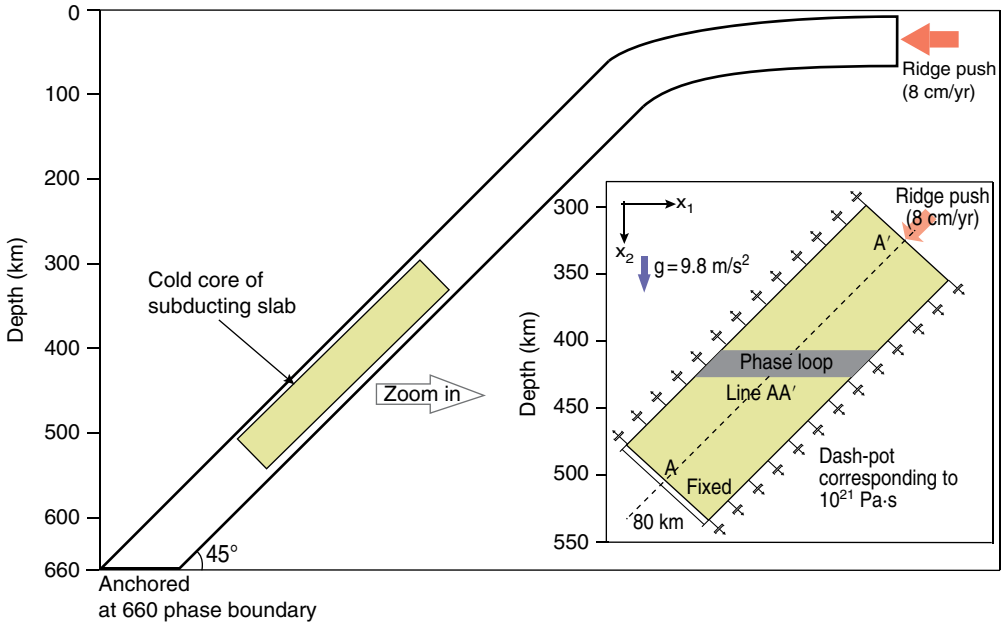

Figure 8.1 The description of the domain for our calculations. We select the cold core of the oceanic lithosphere in a subducting slab with a 45° angle. In the left box, the zoomed domain is shown. The domain (390-km long × 80-km thick) contains the phase loop (25-km thick) with a different shear modulus compared to the surrounding region. The dash-pot elements, which act as an isotactic restoring force from the asthenosphere with a viscosity of 10^{21}Pa·s [*Regenauer-Lieb et al.*, 2001], are set along the right- and left-side boundaries.

8.2. NUMERICAL METHOD AND MODEL SETTINGS

We have performed two-dimensional finite element simulation using ABAQUS code [*Hibbitt, Karlsson and Sorensen, Inc*., 2009]. Because the focus of this study is on the evolution of the thermal structure around the 410-km phase boundary, the domain of our calculation is the cold core of the entire subducting lithosphere containing the phase loop (see Figure 8.1). The depth range of the domain is 275 km–530 km, and the thickness is 80 km. The phase loop and the rest region are respectively meshed by rectangular elements with different sizes of 0.5×0.5 km^2 and 1×1 km^2. The phase loop has a much finer resolution, because the instability is expected to appear around the loop. The angle of subduction is 45°. The lithosphere has an elastoplastic rheology under the assumption of plane strain. Mass, momentum, and energy are conserved within the numerical scheme during the calculation. Continuity, objective derivative of the stress tensor, and energy conservation are described by the following equations (8.1–8.3):

$$\frac{\partial v_i}{\partial x_i} = 0, \tag{8.1}$$

$$\frac{\partial \sigma_{ij}}{\partial x_j} = -\rho g_i, \tag{8.2}$$

and

$$\rho C_P \frac{DT}{Dt} = \rho C_P \left[\frac{\partial T}{\partial t} + v_i \frac{\partial T}{\partial x_i} \right] = \frac{\partial}{\partial x_j} \left(k \frac{\partial T}{\partial x_j} \right) + \tau_{ij} \dot{\varepsilon}_{ij}^{plastic}. \tag{8.3}$$

x_i, v_i, and g_i represent the spatial coordinate, velocity, and gravitational acceleration in the i-th direction, respectively. The g_1 is zero and g_2 is 9.8 m/s^2. ρ, C_P, and k density, specific heat and thermal conductivity, respectively. The σ_{ij} is the total stress tensor, which is the sum of the deviatoric stress tensor (τ_{ij}) and pressure (P) (see equation 8.4).

$$\sigma_{ij} = -P\delta_{ij} + \tau_{ij} \quad \text{where } \delta_{ij} \text{ is the Kronecker delta.} \tag{8.4}$$

D/Dt is the material derivative. The meaning and value of each variable are shown in Table 8.1. In equation 8.3, the last term on the right-hand side is the shear heating, which refers to the conversion of stored elastic energy into thermal energy. Once thermal energy appears, the system goes into a mode involving highly nonlinear feedback among lithospheric plastic strength, plastic strain-rate deformation and shear heating. The total strain-rate ($\dot{\varepsilon}_{ij}^{total}$) is mathematically assumed to be the sum of the elastic ($\dot{\varepsilon}_{ij}^{elastic}$) and plastic ($\dot{\varepsilon}_{ij}^{plastic}$) strain-rates [e.g., *So and Yuen*, 2014]:

$$\dot{\varepsilon}_{ij}^{total} = \dot{\varepsilon}_{ij}^{elastic} + \dot{\varepsilon}_{ij}^{plastic} \tag{8.5}$$

where $\dot{\varepsilon}_{ij}^{total} = \frac{1}{2}\left[\frac{\partial v_i}{\partial x_j} + \frac{\partial v_j}{\partial x_i} \right]$ and $\dot{\varepsilon}_{ij}^{elastic} = \frac{1}{2G} \frac{D\tau_{ij}}{Dt}$.

G refers to the elastic shear modulus. For a simple von Mises yielding criterion (see equation 8.6), the plastic strain-rate will begin and follow the plastic creeping law from experimental studies dealing with olivine (see equation 8.7) [*Chopra and Paterson*, 1981]:

$$J_2 \geq \sigma_{yield} \tag{8.6}$$

and

$$\dot{\varepsilon}_{ij}^{plastic} = A J_2^{n-1} \tau_{ij} \exp\left(-\frac{E^* + PV^*}{RT} \right) \tag{8.7}$$

where $J_2 = \left(\frac{1}{2} \tau_{ij} \tau_{ij} \right)^{1/2}$.

E^* and V^* are the activation energy and activation volume, respectively. E^* can be effectively reduced by the content of water [e.g., *Yoshino et al*., 2006]. Although the basic value of σ_{yield} is 100 MPa, we will test some cases with different values of σ_{yield}, from 10 MPa to 300 MPa.

Once the slab reaches the 660-km phase boundary related to wadsleyite → perovskite + magnesiowüstite [*Ringwood*, 1991], the sinking of the slab into the lower mantle is prevented due to the negative Clapeyron slope at the phase boundary [e.g., *Schubert et al*., 1975; *Ito and Takahashi*, 1989]. For this reason, the stress regime of the slab is down-dip compression in seismological [e.g., *Isacks and Molnar*, 1971] and numerical studies [e.g., *Stadler et al*., 2012]. Following these examples, the bottom and top

Table 8.1 Descriptions of input parameters

Symbol	Values [Unit]	Descriptions
ρ	3300 [kg/m^3]	Density
c_P	900 [J/(kg·K)]	Specific heat
G_{sur}	4×10^{10} [Pa]	Shear modulus outside of the phase loop
σ_{yield}	10-300 [MPa]	Von Mises' yield strength
n	4.48	Power law exponent
A_{litho}	5.5×10^{-25} [Pa^{-n}·s^{-1}]	Prefactor
R	8.314 [J/(K·mol)]	Universal gas constant
E^*	350 [kJ/mol]	Activation energy
V^*	14×10^{-6} [m^3/mol]	Activation volume

Source: *Karato and Ogawa* [1982].

boundary conditions are fixed and constant compressional rate (i.e., 8 cm/yr), respectively. The dash-pot elements, which act as an isostatic restoring force from the purely viscous asthenosphere with a viscosity of 10^{21} Pa·s [*Regenauer-Lieb et al*., 2001], are imposed along the two lateral boundaries. We checked that the viscous dissipation by the dash-pot element is negligibly small, compared with the heating in the phase loop. If we adopt a power-law viscosity into the mantle, the viscous dissipation will be stronger [e.g., *Gerya et al*., 2004].

The formation of the phase loop, which has a lower elastic shear modulus than the surrounding region, is a complicated process because it simultaneously depends on temperature, pressure, and rate of subduction. We can estimate that the phase loop exists at the depth range between 350 km and 450 km with a thickness of 10 km–100 km [*Rubie and Ross II*, 1994]. The cold subducting slab (i.e., old lithosphere and fast subduction) has a thicker and deeper phase loop because the phase transition is kinetically hindered in lower temperature environments. We have predefined a simple and representative phase loop with a 25-km thickness at the depth of 410 km (see Figure 8.1). The fractions of high-pressure polymorph in the phase loop are definitely 0 and 1 at the top and bottom of the loop, respectively [*Rubie and Ross II*, 1994; *So and Yuen*, 2015]. We therefore assumed a quadratic distribution of the shear modulus with the minimum shear modulus at the center of the loop (see Figure 8.1). The contrast of shear moduli (R_s) is varied from 1 to 5 for each calculation to determine the thermal-mechanical effects of elastic lateral heterogeneity on the thermal state of the slab structure.

Because the domain of interest lies in the cold portion of the slab, the distribution of the initial temperature is simply linear from 400°C at the top to 650°C at the bottom (see Figure 8.1), according to the temperature distribution using variable thermal conductivity derived by *Emmerson and McKenzie* [2007]. In addition, the right and left boundaries are thermally insulated. The heat transport through the interface between the cold core and the hot shell can be retarded because of the contrasts in thermal conductivity due to the large difference in the temperature [e.g., *van den Berg et al*., 2004; *Maierová et al*., 2012; *So and Yuen*, 2013].

8.3. RESULTS

First, we will compare the cases of $R_s = 1$ and 3. The case of $R_s = 1$ represents the model where the whole domain has a homogeneous distribution for the shear modulus (i.e., no phase loop and no shear modulus contrast). The case of $R_s = 3$ means that we predefined a quadratic distribution of the shear modulus with a minimum value of 1.33×10^{10} Pa for the loop, and the rest of the domain has a shear

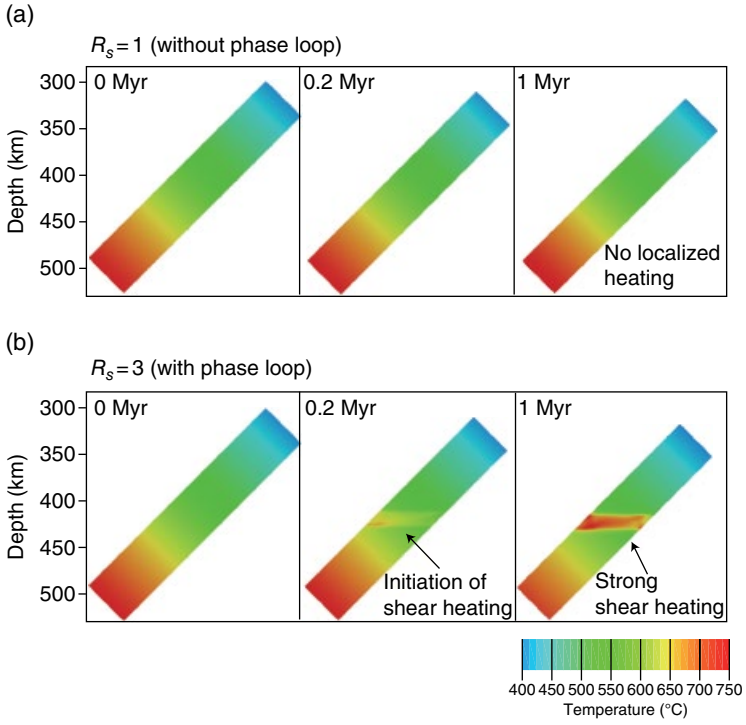

Figure 8.2 (a)The temperature distribution without the phase loop (i.e., $R_s = 1$). No localized shear heating is generated, and no notable high-temperature zone is shown. (b)The temperature distribution with the phase loop (i.e., $R_s = 3$). The heat is narrowly localized around the phase loop.

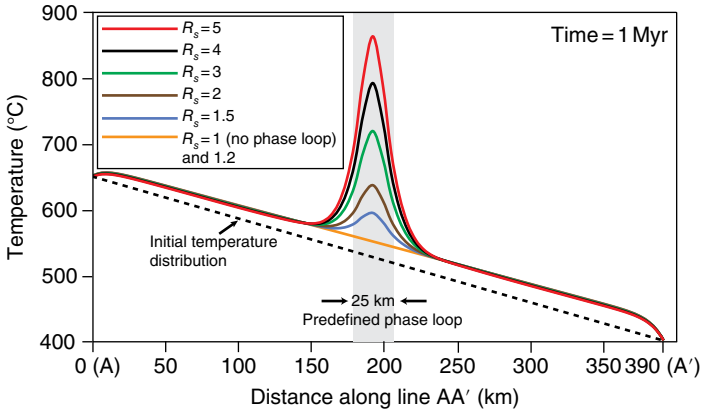

Figure 8.3 Temperature distributions along line AA′ with varying R_s. In the case of larger R_s, the temperature elevation is larger than for smaller R_s. To reduce the deviatoric stress around the phase loop, R_s should be larger than 2 with 1 Myr compression.

modulus of 4×10^{10} Pa. Figures 8.2a–b show the thermal structure without and with the phase loop. No localized shear zone is formed in the case of $R_s = 1$ (see Figure 8.2a). Although more compression is applied, the localized shear zone is not shown, rather broadly distributed temperature increases are observed. Plastic yielding also occurs in the elastically homogeneous model. However, shear heating cannot be so narrowly confined, and, therefore, the heating does not significantly impact the state of deviatoric stress in subducting slabs. This is consistent with results from previous studies dealing with shear instability at the bimaterial interface [e.g., *Langer et al.*, 2010]. On the other hand, the model with the phase loop exhibits a clear localized shear zone around the loop (see Figure 8.2b). In the phase loop, the small temperature perturbation is generated after deforming for 0.2 Myr shortening. When more compression is exerted, the heating enhances and is localized around the loop. The temperature at the center of the loop is ~100°C higher than that at the lower end of the domain. We can observe a slight increase in temperature outside the loop. However, most of the heat is focused inside the loop, which is mechanically weakened enough to generate the positive feedback between the strain and intense localized heating.

The decrease in elastic modulus in the phase loop requires further study because the phase loop is a complicated system that contains many types of minerals as well as olivine and wadsleyite. To consider the uncertainty in the decrease of the shear modulus, we adopt many values of R_s (i.e., from 1 to 5) to test various cases. The activation energy, which is an important factor in determining the magnitude of shear heating, is held constant at 350 kJ/mole for all models. Figure 8.3 shows the temperature increases along Line AA′ with different values of R_s. Very little shear heating is generated in cases with $R_s = 1$, 1.2, and 1.5 (see the orange and blue lines in Figure 8.3). In the case of $R_s < \sim 1.5$, the temperature distribution is similar to that with no phase loop. When R_s is greater than 2, the temperature in the phase loop increases by 100–300°C at 1 Myr. We can predict that the deviatoric stress is significantly reduced around the phase loop. This may have an implication for the ASZ between 300-km and 450-km deep, which is revealed by earthquake distribution.

Mechanical strength plays a strong role in seismic activities. When weakening of the mechanical strength strongly interacts with the heat dissipation, the accumulated mechanical energy is not large enough to release large seismicity. For this reason, we investigate the evolution of mechanical strength with various R_s. The average values of stress over the phase loop under different R_s are calculated. We plotted the deformation time versus the areal average stress in Figure 8.4a. The larger R_s is, the more efficient weakening of strength occurs in the phase loop. The difference in strength between $R_s = 1.5$ and $R_s = 5$ is almost 30% at 1 Myr. Figure 8.4b shows the relation between strain and areal average stress over the phase loop. In phase loops with larger R_s, a larger amount of elastic energy is stored in the loop. The gray shaded areas under each curve in Figure 8.4b indicates the accumulated elastic energy before plastic yielding. This implies that phase loops with smaller shear moduli (i.e., larger R_s) can store more elastic energy. The zone with a larger elastic energy density is more likely to emit efficiently energy in the form of intense shear heating [*Regenauer-Lieb et al.*, 2012]. In Figure 8.4a–b, the level of maximum stress in subducting slabs is ~0.6 GPa, and the stress drop during the heat dissipation is ~0.3 GPa. In previous numerical studies, ~1 GPa has been proposed as an average stress level in subducting slabs [e.g., *Čížková et al.*, 2002; *John et al.*, 2009]. The estimated stress drop based on paleo-earthquake data can go up to ~0.6 GPa [*Andersen et al.*, 2008]. On the other hand, a lower stress level of ~0.1 GPa was calculated using seismic source parameters [*Prieto et al.*, 2013]. Therefore, we found that

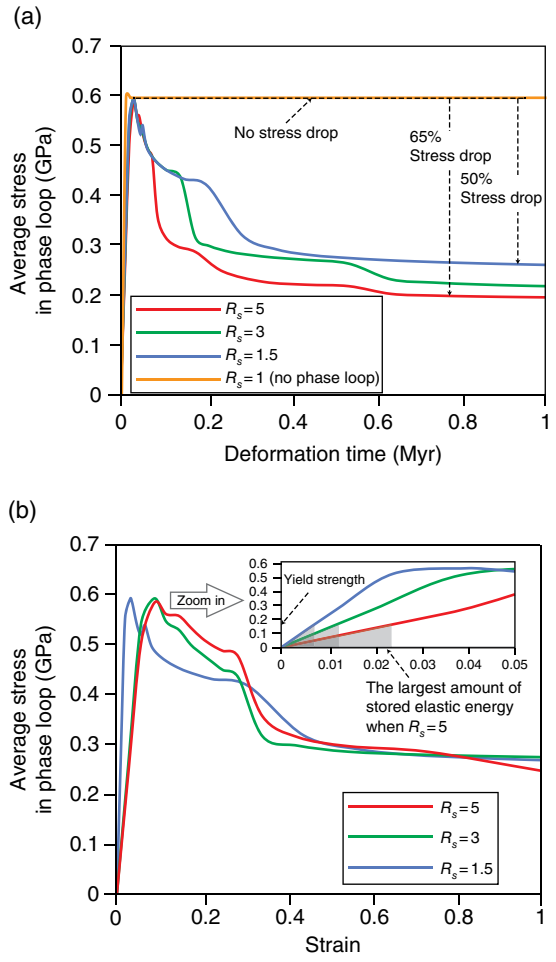

Figure 8.4 (a) Time-varying areal average of stress over the phase loop with different R_s. More efficient weakening occurs in the case of larger R_s than for smaller ones. The weakened phase loop will show weak seismicity. (b) Areal average of stress with strain. Before plastic yielding, larger R_s stores more elastic energy than smaller R_s. This difference in the accumulated elastic energy will influence the thermal structure and the deformation regime after yielding (see gray shaded area in b).

the stress level of the present study lies within the results from previous works. The average values of stress along line AA′ with different R_s are plotted after 1 Myr of deformation (see Figure 8.5). Around the phase loop, the significant drop of stress is shown when large R_s is assigned. On the other hand, the stress drop far from the loop is small. This indicates that the phase loop is not a preferable condition for transformational faulting, which can cause DFEs. In the region near point A, all cases are showing the stress drop, which is caused by the fixed boundary condition.

In order to confirm the relationship between the stored elastic energy density and the amount of dissipation, we plot the time variation of stored elastic energy density in the phase loop. The case of larger R_s can accumulate a

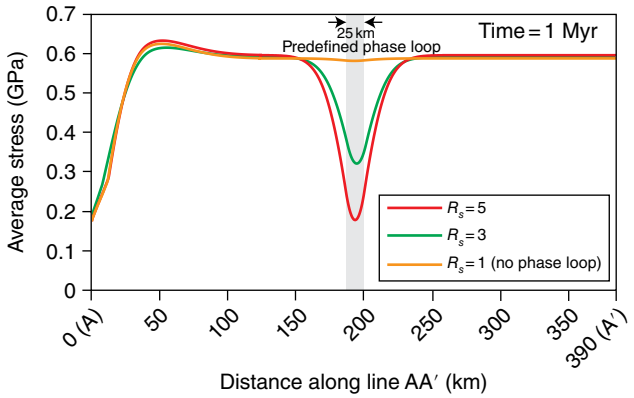

Figure 8.5 The average values of stress along line AA′ with different R_s at 1 Myr deformation. The stress drop around the phase loop is much larger than that far from the loop.

larger amount of elastic energy. After plastic yielding, all phase loops with various values of R_s begin to release the elastic energy (see Figure 8.6a). Apparently, the case with R_s = 5 shows the greatest reduction of elastic energy density within the loop. On the other hand, the surrounding part of the phase loop shows a small amount of elastic energy storage. Moreover, the energy release is very weak (see Figure 8.6b). This indicates that the imbalance of elastic energy densities between the phase loop and the surrounding part cause the significantly concentrated shear heating on the phase loop.

We trace the shear strain along line AA′ for varying R_s in Figure 8.7. The deviatoric stress can enhance the differential movement with attendant shear heating at this depth and lead to the stress drop transforming the deformation regime into rapid aseismic ductile creep [*Ide et al.*, 2007]. The intensively localized negative shear strain in the phase loop is shown. Moreover, the larger R_s induces larger shear strain differences. Each curve of shear strains seems to have two portions. One is the localized shear strain in the phase loop. The other is the strain related with a simple buckling by a compressional boundary condition, and has a small finite amplitude. For the case of R_s = 1 (see the orange line in Figure 8.7), a buckling instability over a whole domain is not generated because of a homogeneous strength of the domain. We also tested the effect of predefined plastic yield strength. Since the yield strength, as well as the elastic heterogeneity, can decide the amount of stored elastic energy, the yield strength may control long-term and global-scale shear heating dissipation. We fixed the R_s at 3, then varied the yield strength from 10 MPa to 300 MPa. Figure 8.8 shows the temperature distribution along line AA′ (see Figure 8.1) after the deformation of 1 Myr with varying the predefined plastic strength. The cases with unrealistically low (i.e., 10 MPa) yield strength, compared with the value derived from laboratory experiments [*Byerlee*,

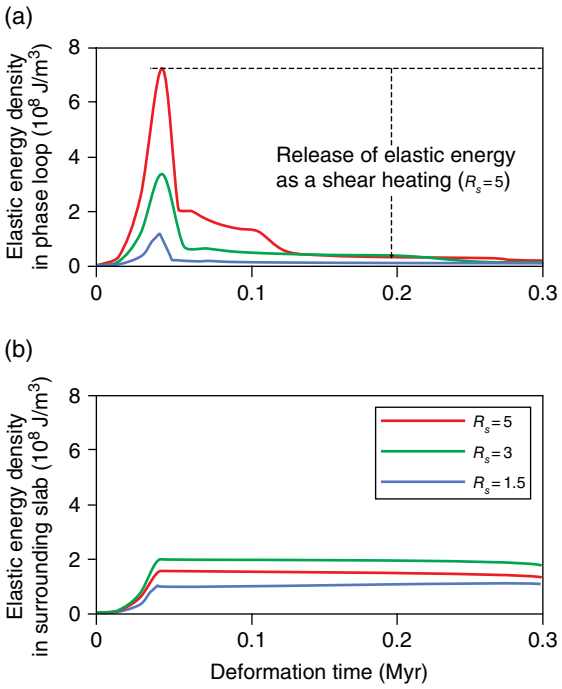

Figure 8.6 (a) The time evolution of elastic energy density in the phase loop. The case of larger R_s accumulates the larger amount of elastic energy. After plastic yielding (see the dotted arrow), the drop of elastic energy is the biggest in the case of the R_s = 5. (b) The time evolution of elastic energy density in the surrounding part. A much smaller amount of elastic energy is stored.

1978], do not show an appropriate thermal structure for the efficient stress drop around the 410-km phase boundary. The cases for 10 MPa show the broadly distributed temperature increase, which is similar with the case of small R_s. The absolute amount of elastic energy in cases with lower yield strength is too low to trigger off the bimaterial instability and promote it to a matured shear zone. The case of 300 MPa yield strength induced the broad and large temperature increase without the localized thermal structure (see the black solid line in Figure 8.8). Due to large yield strength, the outside region of the phase loop accumulates enough elastic strain energy, and then releases large thermal energy, as much as the phase loop does. On the other hand, a localized shear zone is clearly observable in the cases of realistic yield strength (i.e., from 100 to 200 MPa) [*Byerlee*, 1978]. We may deduce that the important factor for efficient shear localization is not only a large enough R_s but also a suitable range of yield strength.

8.4. DISCUSSION

We have attempted to verify our hypothesis that the shear heating from bimaterial interface due to the existence of the phase loop may be able to explain why there is weak seismicity in the depth range between 300 km and 450 km in subducting slabs. We showed that a large deviatoric stress drop occurs in the ASZ (i.e., 300–450 km

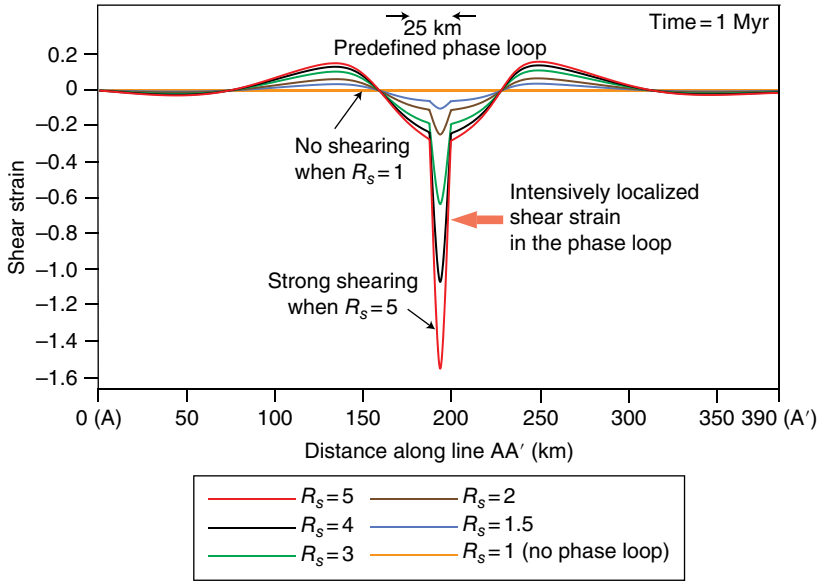

Figure 8.7 The shear strain along line AA′ with varying R_s. When a larger R_s is adopted, the stress difference between the loop and the surrounding areas is greater. This means that the positive feedback with shear heating in cases of larger R_s is stronger. This is a more conducive environment for the deviatoric stress drop, which can restrict the transformational faulting and the subsequent DFEs.

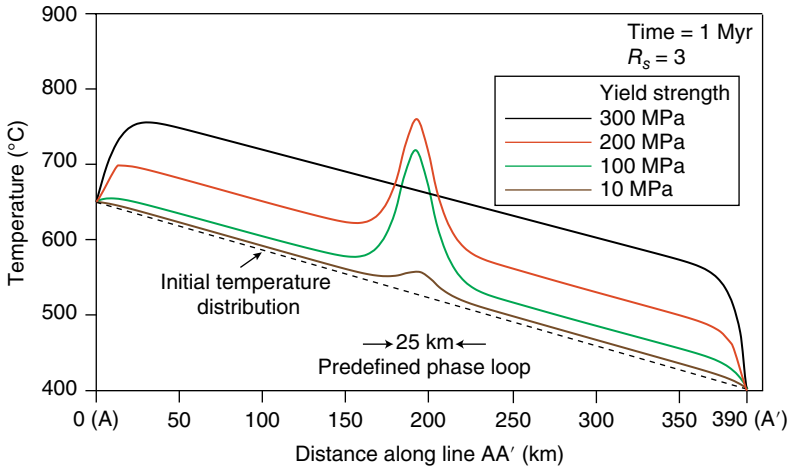

Figure 8.8 Temperature distributions along line AA′ with varying yield strengths. In the case of small yield strength (i.e., 10 and 50 MPa), the temperature distribution does not exhibit well-localized structure due to a small elastic energy accumulation. For the case of unrealistically large yield strength (i.e., 300 MPa), the localized thermal structure does not appear. The only range between 100 and 200 MPa generates localized shear heating, which can selectively reduce the deviatoric stress level.

depth) by the shear heating and strain softening when the shear modulus sufficiently decreases in the phase loop. Many studies have expended much effort to constrain the thermal structure and the stress distribution of the subducting slab. For instance, *Emmerson and McKenzie* [2007] proposed that the low temperature (<~600°C) in the cold core of the subducting slab can persist down to a depth of 660 km because of temperature-dependent thermal conductivity, which can retard heat diffusion from the hot mantle to the cold slab. Even though they were successful in explaining the existence of DFEs at levels deeper than 450 km, their models did not consider how the ASZ is formed at depths between 300 km and 450 km. *Ogawa* [1987] also discussed one of the most important factors for triggering DFEs. He argued that the shear melting of slab materials is followed by seismic slip. However, the mechanism for the ASZ was not taken into account.

Although a couple of hypotheses based on shear heating are frequently adopted for geodynamical situations in Earth's near-surface such as folding instability [e.g., *Hobbs et al*., 2007] and the initiation of subduction [e.g., *Regenauer-Lieb et al*., 2001], the shear heating from a bimaterial interface (i.e., phase loop) is first applied in modeling of deep subduction dynamics. It is because the elasticity has been thought to be ignored in a long timescale geodynamics due to the short timescale physics of viscoelasticity. Some have argued the importance of elasticity in short timescale geodynamical phenomena such as the slip behavior [*Weertman*, 1980] and vibration at the fault plane [*Adams*, 1995]. However, few studies have focused on the elastic energy storage in the embedded zone with lower elastic modulus. Especially, *Kaus and Becker* [2007] argued that the elasticity contrast does not significantly affect Rayleigh-Taylor instability in mantle convection. Their elastic contrast was given for just long wavelength undulation, which is not the suitable contrast for the viscous dissipation by short wavelength localized elastic energy accumulation. On the contrary, we have shown that the short wavelength elastic heterogeneity in the slab can induce a localized shear heating, which can strongly influence the stress level of the slab. However, the problem of our study is that the shear modulus reduction in the phase loop has not been seismically detected but rather has been observed in laboratory experiments [*Li and Weidner*, 2008]. Since the expected depth of phase loop is too deep and its thickness is on the order of tens of kilometers, it is difficult that the loop is seismically detected [*Ricard et al*., 2009]. With a consideration of the impact of bimaterial shear instability near the Earth's surface such as asymmetric mechanical rupture propagation and the distribution of aftershocks in geophysical [e.g., *Rubin and Gillard*, 2000] and numerical studies [e.g., *Dalguer and Day*, 2009], we should consider the localized bimaterial effect on the slab dynamics. According to recent experimental and semitheoretical studies [*Li and Weidner*, 2008; *Ricard et al*., 2009], the attenuation of the shear velocity is ~40%, which refers to ~70% decrease in the elastic modulus. In our study, the cases of small R_s (< ~1.5) do not show strong shear heating to cause a large drop in deviatoric stress. On the other hand, for cases of R_s greater than 2, the shear heating is sufficiently large to cause the stress drop. For instance,

So et al. [2012], in their numerical study, found that a critical R_s value (i.e. ~1.7) for triggering an asymmetric shear instability. In seismological observations, the asymmetric features of aftershocks [*Rubin and Gillard*, 2000] and the patterns of damage [*Dor et al*., 2006] along the San Andreas faults appear at the boundary between the Pacific and North American plates, which is intrinsically a bimaterial interface. The seismic velocity in the stiff Pacific plate is 20% faster than that in the compliant North American plates [e.g., *Eberhart-Phillips and Michael*, 1998; *Allam and Ben-Zion*, 2012], which corresponds to R_s = ~1.5.

We also investigated the elastic energy stored in the phase loop before plastic yielding and the strength of the loop after plastic yielding. *Regenauer-Lieb et al*. [2012] argued that lithospheres with lower elastic moduli, which accumulate larger elastic strain energies before the yielding, can more strongly influence the long-term evolution of thermal and mechanical structures than those with higher elastic moduli. We found that the stored elastic energy in the loop is much larger due to the larger strain associated with greater values of R_s. The loop with a larger amount of stored elastic energy more easily dissipates the energy as a form of shear heating. Another important issue is the contrast in plastic yield strength. Since we fixed the yield strength to be the same for both the phase loop and the surrounding region, the contrast in elastic modulus mainly controls the amount of elastic energy in the loop. If we use different yield strengths for the loop and surrounding region, the stored elastic energy is simultaneously controlled by the contrasts in the yield strength and the elastic modulus. Even though the yield strength of rocks has been thought to be similar regardless of types of rock, a slight difference in the yield strength from type of rock, water contents, and temperature can induce a very contrasting rheological behavior in geological timescale.

In addition to the bimaterial interface caused by the phase loop in the subducting slab, the bimaterial condition is commonplace in natural geomaterials at various spatial scales, such as the grain, glacial, fault, and plate boundary scales [*Lutter et al*., 2004; *Deichmann et al*., 2000], and should be considered in studies involving short wavelength shear instability. In spite of the importance and relevance of the elastic heterogeneity, few numerical studies have applied the elastic heterogeneity within the subducting slab and other geological situations. However, we have produced a distinct result by adopting the phase loop in the subducting slab. The complicated system of subducting slabs includes other bimaterial interfaces, and these interfaces have the potential to cause shear heating according to the mechanism we have discussed. We have not considered the time evolution of thermal energy with chemical reactions. For instance, dehydration of hydrous mineral is a strong endothermic reaction. If we implemented the process of dehydration in our study, the temperature increase within the phase loop could be smaller, because the heat energy must be consumed by the dehydration [*Veveakis et al*., 2010]. Moreover, the enhanced dehydration by shear heating can cause DFEs [*Green et al*., 2010]. Therefore, we should further investigate the relationship between the shear heating and endothermic dehydration reaction.

8.5. CONCLUSIONS

The ASZ is a region of great interest because it is located between two seismically active zones. With subduction toward the deep mantle, the pressure and temperature of the slab must be elevated; thus, the deformation regime of the deeper parts should be more aseismic. However, the ASZ is more aseismic than the hotter lower part of the slab. Since low- and high-pressure polymorphs (i.e., olivine and spinel, respectively) simultaneously exist, the olivine-spinel phase transition usually occurs around the 410-km phase boundary. This indicates that the DFEs with transformational faulting should occur. However, just a small number of DFE activity is recorded. The necessary condition for effective transformational faulting is a large deviatoric stress. Thus, in this study, we have suggested that additional mechanisms may decrease the deviatoric stress level, and then the ASZ appears around the phase loop by applying recent results regarding bimaterial instability and the 410-km phase loop.

The bimaterial interface due to the phase loop, which is the coexistence zone of lower and higher pressure polymorphs and has a lower shear modulus, results in the storage of dense elastic energy and strong shear heating for the deviatoric stress drop. Models containing a phase loop with R_s > ~2 showed a sufficient stress drop (i.e., ~500 MPa) due to the bimaterial shear heating. This shear heating can induce the ASZ around the phase loop. This explanation may be a new approach for the ASZ inside subducting slabs. Moreover, the pressure-induced amorphous zone also has a low shear modulus [e.g., *Binggeli et al*., 1994]. Both the phase loop and the amorphized zone can act in concert as a bimaterial interface, thus influencing the thermal-mechanical structure of the slab. Hence, observational constraints of these elastic heterogeneities in the slab should be investigated. Finally, we should apply in the future the elastic contrast to explain the ASZ and buckling inside the subducting slab. Moreover, recent studies suggested [e.g., *Gerya*, 2015; *Schmalholz and Duretz*, 2015; *So and Yuen*, 2015] that the pressure deviation from lithostatic pressure (i.e., tectonic over-pressure and under-pressure) after the plastic yielding can affect the pressure-temperature condition and mechanical behaviors of deforming lithosphere.

ACKNOWLEDGMENT

We acknowledge with thanks our discussions with Shun-ichiro Karato and constructive comments by an anonymous reviewer and Manolis Veveakis. This work was supported by the National Research Foundation of Korea (NRF) grants funded by the Korean government (NRF-2014R1A6A3A04055841) for B.-D. So and by U.S. National Science Foundation grants in the Collaboration of Mathematics and Geosciences (CMG) program and Geochemistry for D. A. Yuen.

REFERENCES

Adams, G. G. (1995), Self-excited oscillations of two elastic half-spaces sliding with a constant coefficient of friction, *J. Appl. Mech.*, *62*, 867–872.

Andersen, T. B., K. Mair, H. Austrheim, Y. Y. Podladchikov, and J. C. Vrijmoed (2008), Stress-release in exhumed intermediate-deep earthquakes determined from ultramafic pseudotachylyte, *Geology*, *36*, 995–998.

Allam, A. A., and Y. Ben-Zion (2012), Seismic velocity structures in the southern California plate-boundary environment from double-difference tomography, *Geophys. J. Int.*, *190*(2), 1181–1196.

Ampuero, J.-P, and Y. Ben-Zion (2008), Cracks, pulses and macroscopic asymmetry of dynamic rupture on a biomaterial interface with velocity-weakening friction, *Geophys. J. Int.*, *173*, 674–692, doi: 10.1111/j.1365-246X.2008.03736.x.

Ben-Zion, Y., and Z. Shi (2005), Dynamic rupture on a material interface with spontaneous generation of plastic strain in the bulk, *Earth Planet. Sci. Lett.*, *236*(1–2), 486–496.

Binggeli, N., N. R. Keskar, and J. R. Chelikowsky (1994), Pressure-induced amorphization, elastic instability, and soft modes in a-quartz, *Phys. Rev. B*, *49*, 3075–3081.

Byerlee, J. D. (1978), Friction of rock, *Pure Appl. Geophys.*, *116*(4–5), 615–626.

Chen, Y., and L. Wen (2015), Global large deep-focus earthquakes: Source process and cascading failure of shear instability as a unified physical mechanism, *Earth and Planet. Sci. Lett., 423*, 134–144, doi:10.1016/j.epsl.2015.04.031

Chopra, P. N., and M. S. Paterson (1981), The experimental deformation of dunite, *Tectonophysics*, *78*(1–4), 453–473.

Čížková, H., J. van Hunen, A. P. van den Berg, and N. J. Vlaar (2002), The influence of rheological weakening and yield stress on the interaction of slabs with the 670 km discontinuity, *Earth Planet. Sci. Lett.*, *199*, 447–457.

Dalguer, L. A., and S. M. Day (2009), Asymmetric rupture of large aspect ratio faults at bimaterial interface in 3D, *Geophys. Res. Lett.*, *36*, L23307, doi:10.1029/2009GL040303.

Deichmann, N., J. Ansorge, F. Scherbaum, A. Aschwanden, F. Bernardi, and G. H. Gudmundsson (2000), Evidence for deep icequakes in an Alpine glacier, *Ann. Glac.*, *31*, 85–90, doi: 10.3189/172756400781820462.

Dor, O., T. K. Rockwell, and Y. Ben-Zion (2006), Geological observations of damage asymmetry in the structure of the San Jacinto, San Andreas and Punchbowl faults in Southern California: A possible indicator for preferred rupture propagation direction, *Pure Appl. Geophys.*, *163*, 301–349.

Eberhart-Phillips, D., and, A. J. Michael (1998), Seismotectonics of the Loma Prieta, California region determined from three-dimensional *Vp*, *Vp*/*Vs*, and seismicity, *J. Geophys. Res.*, *103*, 21099–21120.

Emmerson, B., and D. McKenzie (2007), Thermal structure and seismicity of subducting lithosphere, *Phys. Earth Planet. Inter.*, *163*, 191–208.

Frohlich, C. (2006), *Deep Earthquakes*, Cambridge Univ. Press, Cambridge, UK.

Fukao, Y., S. Widiyantoro, and M. Obayashi (2001), Stagnant slabs in the upper and lower mantle transition region, *Rev. Geophys.*, *39*(3), 291–323.

Gerya, T. V., D. A. Yuen, and W. V. Maresch (2004), Thermomechanical modelling of slab detachment, *Earth Planet. Sci. Lett.*, *226*(1–2), 101–106.

Green, H., and P. C. Brunley (1989), A new self-organizing mechanism for deep-focus earthquakes, *Nature*, *341*(6244), 733–737, doi:10.1038/341733a0.

Green, H. W., W.-P. Chen, and M. R. Brudzinski (2010), Seismic evidence of negligible water carried below 400-km depth in subducting lithosphere, *Nature*, *467*, 828–831.

Hibbitt, Karlsson & Sorensen, Inc. (2009), *Abaqus*/*Standard User's Manual Version 6.9*, Pawtucket, RI.

Hobbs, B., K. Regenauer-Lieb, and A. Ord (2007), Thermodynamics of folding in the middle to lower crust, *Geology*, *35*, 175–178, doi:10.1130/G23188A.

Houston, H. (2007), *Deep Earthquakes*, in G. Schubert (ed.), *Treatise on Geophysics, 4. Earthquake Seismology*, Elsevier, Amsterdam, 321–350.

Ide, S., G. C. Beroza, D. R. Shelly, and T. Uchide (2007), A scaling law for slow earthquakes, *Nature*, *447*, 76–79, doi:10.1038/nature05780.

Iidaka, T., and D. Suetsugu (1992), Seismological evidence for metastable olivine inside a subducting slab, *Nature*, *356*, 593–595.

Isacks, B., and P. Molnar (1971), Distribution of stress in descending lithosphere from a global survey of focal-mechanism solutions of mantle, earthquakes, *Rev. Geophys.*, *9*, 103–174.

Isacks, B., J. Oliver, and L. R. Sykes (1968), Seismology and the new global tectonics, *J. geophys. Res.*, *73*, 5855–5899.

Ito, E., and E. Takahashi (1989), Postspinel transformations in the system Mg_2SiO_4–Fe_2SiO_4 and some geophysical implications, *J. Geophys. Res.*, *91*, 10637–10646.

Jackson, D. D., and D. L. Anderson (1970), Physical mechanisms of seismic-wave attenuation. *Rev. Geophys. Space Phys.*, *8*, 1–63.

Ji, S., and M. H. Salisbury (1993), Shear-wave velocities, anisotropy and splitting in high-grade mylonites, *Tectonophysics*, *221*, 453–473.

John, T., S. Medvedev, L. H. Rüpke, T. B. Andersen, Y. Y. Podladchikov, and H. Austrheim (2009), Generation of intermediate-depth earthquakes by self-localizing thermal runaway, *Nat. Geosci.*, *2*, 137–140, doi:10.1038/ngeo419.

Jung, H., H. W. Green, and L. F. Dobrzhinetskaya (2004), Intermediate-depth earthquake faulting by dehydration embrittlement with negative volume change, *Nature*, *428*(6982), 545–549.

Karato, S., and M. Ogawa (1982), High-pressure recovery of olivine: implications for creep mechanisms and creep activation volume, *Phys. Earth Planet. Inter.*, *28*(2), 102–117.

Kaus, B. J. P., and T. W. Becker (2007), Effects of elasticity on the Rayleigh–Taylor instability: Implications for large-scale geodynamics, *Geophys. J. Int.*, *168*(2), 843–862, doi:10.1111/j.1365-246X.2006.03201.x.

Kirby, S. H., S. Stein, E. A. Okal, and D. C. Rubie (1996), Metastable mantle transformations and deep earthquakes in subducting oceanic lithosphere, *Rev. Geophys.*, *34*, 261–306.

Langer, S., L. M. Olsen-Kettle, D. K. Weatherley, L. Gross, and H.-B. Mühlhaus (2010), Numerical studies of quasi-static tectonic loading and dynamic rupture of bi-material interfaces, *Concurrency Comput. Pract. Exper.*, *22*(12), 1684–1702, doi: 10.1002/cpe.1540.

Li, L., and D. J. Weidner (2008), Effect of phase transitions on compressional-wave velocities in the Earth's mantle, *Nature*, *454*(7207), 984–986, doi:10.1038/nature07230.

Liu, L., and J. S. Zhang (2015), Differential contraction of subducted lithosphere layers generates deep earthquakes. *Earth and Planet. Sci. Lett.*, *421*, 98–106, doi:10.1016/j.epsl.2015.03.053.

Lutter, W. J., G. S. Fuis, T. Ryberg, D. A. Okaya, R. W. Clayton, P. M. Davis, C. Prodehl, J. M. Murphy, V. E. Langenheim, M. L. Benthien, N. J. Godfrey, N. I. Christensen, K. Thygesen, C. H. Thurber, G. Simila, and G. R. Keller (2004), Upper crustal structure from the Santa Monica mountains to the Sierra Nevada, southern California: tomographic results from the Los Angeles regional seismic experiment, Phase II (LARSE II), *Bull. Seism. Soc. Am.*, *94*(2), 619–632.

Maierová, P., T. Chust, G. Steinle-Neumann, O. Čadek, and H. Čizkova (2012), The effect of variable thermal diffusivity on kinematic models of subduction, *J. Geophys. Res.*, *117*, B07202.

Meade, C., and R. Jeanloz (1991), Deep-focus earthquakes and recycling of water into the Earth's mantle, *Science*, *252*(5002), 68–72.

Myhill, R. (2013), Slab buckling and its effect on the distributions and focal mechanisms of deep-focus earthquakes, *Geophys. J. Int.*, *192*, 837–853.

Ogawa, M. (1987), Shear instability in a viscoelastic material as the cause of deep focus earthquakes, *J. Geophys. Res.*, *92*, 13801–13810, doi:10.1029/JB092iB13p13801.

Peacock, S. M., T. Rushmer, and A. B. Thompson (1994), Partial melting of subducting oceanic crust, *Earth Planet. Sci. Lett.*, *121*(1–2), 227–244.

Prieto, G. A., M. Florez, S. A. Barrett, G. C. Beroza, P. Pedraza, J. F. Blanco, and E. Poveda (2013), Seismic evidence for thermal runaway during intermediate-depth earthquake rupture, *Geophys. Res. Lett.*, *40*(23), 6064–6068.

Regenauer-Lieb, K., D. A. Yuen, and J. Branlund (2001), The initiation of subduction: Criticality by addition of water? *Science*, *294*, 578–581.

Regenauer-Lieb, K., F. Roberto, G. R. Weinberg (2012), The role of elastic stored energy in controlling the long term rheological behaviour of the lithosphere, *J. Geodyn.*, *55*, 66–75.

Ricard, Y., J. Matas, and F. Chambat (2009), Seismic attenuation in a phase change coexistence loop, *Phys. Earth Planet. Inter.*, *176*(1–2), 124–131, doi: 10.1016/j.pepi.2009.04.007.

Ringwood, A. E. (1991), Phase transformations and their bearing on the constitution and dynamics of the mantle, *Geochim. Cosmochim. Acta*, *55*, 2083–2110.

Rubie, D. C., and C. R. Ross II (1994), Kinetics of the olivine-spinel transformation in subducting lithosphere: experimental constraints and implications for deep slab processes, *Phys. Earth Planet. Inter.*, *86*, 223–241.

Rubin, A. M., and D. Gillard (2000), Aftershock asymmetry/rupture directivity among central San Andreas fault microearthquakes, *J. Geophys. Res.*, *105*, 19,095–19,109.

Schmalholz, S. M., and Y. Y. Podladchikov (2013), Tectonic overpressure in weak crustal-scale shear zones and implications for the exhumation of high-pressure rocks, *Geophys. Res. Lett.*, *40*(10), 1984–1988.

Schubert, G., D. A. Yuen, and D. L. Turcotte (1975), Role of phase transitions in a dynamic mantle, *Geophys. J. R. Astron. Soc.*, *42*,705–735.

Schubnel, A., F. Brunet, N. Hilairet, J. Gasc, Y. Wang, and H. W. Green (2013), Deep-focus earthquake analogs recorded at high pressure and temperature in the laboratory, *Science*, *341*(6152), 1377–1380.

So, B.-D., and D. A. Yuen (2014), Stationary points in activation energy for heat dissipated with a power law temperature-dependent viscoelastoplastic rheology, *Geophys. Res. Lett.*, *41*, 4953–4960, doi:10.1002/2014GL060713.

So, B. D. and D. A. Yuen (2015). Generation of tectonic overpressure inside subducting oceanic lithosphere involving phase-loop of olivine–wadsleyite transition, *Earth Planet. Sci. Lett.*, *413*, 59–69, doi:10.1016/j.epsl.2014.12.048.

So, B.-D., and D. A. Yuen (2013), Influences of temperature-dependent thermal conductivity on surface heat flow near major faults, *Geophys. Res. Lett.*, *40*(15), 3868–3872, doi:10.1002/grl.50780.

So, B.-D., D. A. Yuen, K. Regenauer-Lieb, and S.-M. Lee (2012), Asymmetric lithospheric instability facilitated by shear modulus contrast: Implications for shear zones, *Geophys. J. Int.*, *190*(1), 23–36, doi:10.1111/j.1365-246X.2012.05473.x.

Stadler, G., M. Gurnis, C. Burstedde, L. C. Wilcox, L. Alisic, and O. Ghattas (2010), The dynamics of plate tectonics and mantle flow: From local to global scales, *Science*, *329*(5995), 1033–1038, doi:10.1126/science.1191223.

Sung, C. M., and R. G. Burns (1976), Kinetics of high-pressure phase transformations: implications to the evolution of the olivine-spinel transition in the downgoing lithosphere and its consequences on the dynamics of the mantle, *Tectonophysics*, *31*, 1–32.

Sykes, L. R. (1966), The seismicity and deep structure of island arcs, *J. Geophys. Res.*, *71*, 2981–3006.

Tackley, P. J. (1998), Self-consistent generation of tectonic plates in three-dimensional mantle convection, *Earth Planet. Sci. Lett.*, *157*(1–2), 9–22.

van den Berg, A. P., D. A. Yuen, and E. S. G. Rainey (2004), The influence of variable viscosity on delayed cooling due to variable thermal conductivity, *Phys. Earth Planet. Inter.*, *142*, 283–295.

Veveakis, E., S. Alevizos, and I. Vardoulakis (2010), Chemical reaction capping of thermal instabilities during shear of frictional faults, *J. Mech. Phys. Solids*, *58*(9), 1175–1194.

Weertman, J. (1980), Unstable slippage across a fault that separates elastic media of different elastic constant, *J. Geophys. Res.*, *85*(B3), 1455–1461.

Yoshino, T., T. Matsuzaki, S. Yamashita, and T. Katsura (2006), Hydrous olivine unable to account for conductivity anomaly at the top of the asthenosphere, *Nature*, *443*, 973–976, doi:10.1038/nature05223.